MJFAS MALAYSIAN JOURNAL OF FUNDAMENTAL AND APPLIED SCIENCES
PRINT ISSN: 2289-5981 | ONLINE ISSN: 2289-599X

RESEARCH ARTICLE

Imazalil sulphate pesticide degradation using silver loaded hollow anatase TiO_2 under UV light irradiation

Afrouz Baharvand [a], Rusmidah Ali [b], Hadi Nur [c,*]

[a] Centre for Sustainable Nanomaterials, Ibnu Sina Institute for Scientific and Industrial Research, Universiti Teknologi Malaysia, Skudai 81310, Johor, Malaysia
[b] Department of Chemistry, Faculty of Science, Universiti Teknologi Malaysia, 81310 UTM Johor Bahru, Johor, Malaysia

* Corresponding author: hadi@kimia.fs.utm.my

Article history
Received 2 March 2016
Received in revised form 20 May 2016
Accepted 22 May 2016

Graphical abstract

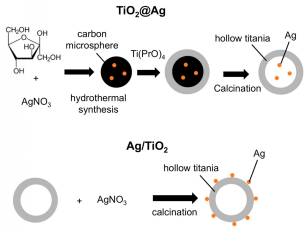

Abstract

Silver loaded hollow anatase TiO_2 particles with the location of silver are inside ($Ag@TiO_2$) and outside (Ag/TiO_2) the hollow TiO_2 structure have been successfully synthesized by a deposition-precipitation and template methods. The effects of silver nanoparticles location on $Ag@TiO_2$ and Ag/TiO_2 has been evaluated in the photodegradation efficiency of imazalil sulphate pesticide in aqueous suspension under ultraviolet irradiation. The Ag/TiO_2 showed better photocatalytic performance for the degradation of imazalil sulphate, compared to $Ag@TiO_2$ and hollow TiO_2 microspheres. A higher photocatalytic activity of Ag/TiO_2 compared to $Ag@TiO_2$ and hollow TiO_2 can be considered as an evidence of enhanced charge separation of Ag/TiO_2 photocatalyst as confirmed by photoluminescence spectroscopy.

Keywords: Silver nanoparticles, hollow anatase TiO_2, imazalil sulphate, UV irradiation, photodegradation

INTRODUCTION

Hollow TiO_2 microspheres are associated with a high surface area, low density, easy recovery, ability to deliver of drugs, high surface permeability (Yu *et al.*, 2007b) and have multiple light reflection and diffraction (Kondo *et al.*, 2007). It is also believed that the structural features also improved its light harvesting ability by allowing more light to penetrate into its interior (Kondo *et al.*, 2007; Li *et al.*, 2007b). This light-harvesting ability makes hollow TiO_2 as promising photocatalyst (Kondo *et al.*, 2007). The photocatalytic activity of TiO_2 is due to the formation of a photo-induced electron and a positive hole which occurs as a result of ultraviolet light absorption which corresponds to the energy gap (Herrmann, 1999). These species are believed to be mobile and are capable of initiating many photocatalytic reactions. However, the fast recombination of photogenerated electrons and holes limits both the photocatalytic efficiency and activity of TiO_2. Therefore, the photocatalytic activity of TiO_2 can be improved by controlling the steps involved during the photocatalysis by TiO_2. These steps include e^- and h^+ generation, followed by their separation, migration and the reaction on the surface with adsorbed species. The photoinduced charge separation in bare TiO_2 particles has a very short lifetime, which is due to the recombination of charges. So, it is vital to prevent electron–hole recombination before a designated chemical reaction occurs on the surface of TiO_2. High recombination rate of the photogenerated electron–hole pairs limit the industrial application of TiO_2. Since charge separation is found to be a major problem, many attempts were made to improve the photocatalytic activity of TiO_2 by modifying the surface or bulk properties. This includes coupling of two semiconductors (Tada *et al.*, 1998), metal deposition (Sclafani and Herrmann, 1998; Seery *et al.*, 2007; Cozzoli *et al.*, 2004; Xu *et al.*, 2005), surface chelation and doping (Xu *et al.*, 2005; Chatterjee and Mahata, 2002; Tada *et al.*, 1998).

The high rate of photogenerated electron–hole pairs recombination process can be minimized by loading metal nanoparticles on the surface of TiO_2 (Subramanian *et al.*, 2004). In this system, photo promoted electrons are captured by noble metal nanoparticles, which have Fermi level energy lower than the conduction band potential of the semiconductor with a consequent increase of the overall photocatalytic efficiency, especially under UV light (Subramanian *et al.*, 2004). Various synthesis approaches have been established to prepare noble metal deposited TiO_2 materials. Those approaches that are generally utilized, including chemical reduction (Tao *et al.*, 2006), impregnation (Behnajady *et al.*, 2008), sol-gel (Lenzi *et al.*, 2011), hydrothermal (Zielińska *et al.*, 2010), microemulsion (Sharma *et al.*, 2009), electrospinning (Abou El-Nour *et al.*, 2010), deposition-precipitation (Subrahmanyam *et al.*, 2012), spray pyrolysis (Zhou *et al.*, 2011) and irradiation (*i.e.*, laser, microwave, radiolysis, etc.) (Grabowska *et al.*, 2013; Sharma *et al.*, 2009).

Although this type of catalyst's structure is effective, metals on the surface of the semiconductor are easily corroded and dissolved (Hirakawa and Kamat, 2005). To overcome these drawbacks, the noble metals are incorporated into the core and the semiconductor, such as TiO_2, acts as the shell (Tom *et al.*, 2003; Ung *et al.*, 1998; Pastoriza-Santos *et al.*, 2000; Chan and Barteau, 2005). Among all of these types of particles, $TiO_2@Ag$ particles have been intensively investigated because of their potential applications in photocatalysis and fabrication of electronic devices (Pastoriza-Santos *et al.*, 2000; Tom *et al.*, 2003; Hirakawa and Kamat, 2004b; Jang *et al.*, 2006).

In the previous paper (Baharvand *et al.*, 2014), we reported the synthesis of hollow anatase TiO_2 microspheres by employing carbon particles as a template. In the present paper, we investigated the functionalization of hollow anatase TiO_2 with Ag nanoparticles inside and outside, with the aim of improving the photocatalytic efficiency. First, two types of noble metal modified hollow anatase TiO_2, such as silver core anatase TiO_2 shell (TiO_2@Ag) and surface modified hollow anatase TiO_2 with silver (Ag/TiO_2) were prepared (see Fig. 1). Second, the effect of modification of hollow TiO_2 with Ag in photocatalytic decomposition of imazalil sulphate pesticide in aqueous medium was investigated. This is the first report in which photocatalytic activities of Ag nanoparticles modified hollow anatase TiO_2 microspheres are examined in the degradation of imazalil sulphate pesticide.

EXPERIMENTAL

Materials

The starting materials, fructose (D-(-)-type, Sigma-Aldrich, 99%), silver nitrate ($AgNO_3$, AR, QRëC^{TM}), titanium tetraisopropoxide (TTIP, Sigma-Aldrich, 97%) and absolute ethanol (EtOH, HmbG® Chemicals) were used as the precursor for carbon microspheres, silver, and TiO_2 microspheres, respectively.

Synthesis of Ag/TiO_2 microspheres

The Ag/TiO_2 microspheres, where the location of Ag nanoparticles are attached on the external surface of hollow TiO_2, were prepared by deposition-precipitation method using urea and previously synthesized hollow anatase TiO_2. The synthesis of hollow TiO_2 spheres is given in details in reference (Baharvand *et al.*, 2014). TiO_2 (0.1 g) was added to a 10 mL aqueous solution containing $AgNO_3$ (Ag 1 wt/wt %) and 0.25 g urea. The suspension was then refluxed at 80 °C and kept at this temperature for 4 h under continuous stirring. The sample was then collected by centrifugation, washed repeatedly with deionized water, dried for 12 h at 80 °C and then calcined at 300 °C for 4 h.

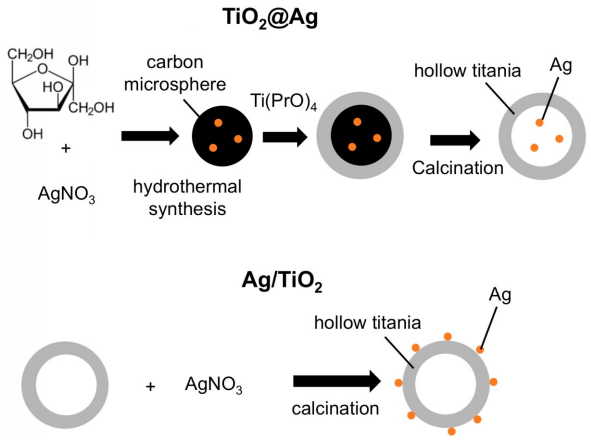

Fig. 1 Schematic diagram for preparation of TiO_2@Ag and Ag/TiO_2 microspheres.

Synthesis of Ag@TiO_2 microspheres

The Ag@TiO_2 particles, silver loaded hollow anatase TiO_2 particles with the location of Ag are inside the hollow TiO_2 structure is by template method. 2.4 mL of aqueous solution $AgNO_3$ was added dropwise into 40 mL of aqueous fructose solution (0.5 M) under vigorous stirring. After stirring for 20 min, the solution was transferred and sealed in a Teflon-sealed autoclave. The autoclave was placed in an oven at 160 °C for 5 h, yielding Ag@C microspheres. 2.6 mL of TTIP was added to a colloidal suspension of Ag@C under vigorous stirring and then the mixture was aged under ambient conditions for one day. The product was collected by centrifugation and washed with ethanol, then dried at 60 °C in an oven. Ag@TiO_2 were finally obtained after the sample was calcined at 600 °C for 3 h in a furnace.

Characterization techniques

The prepared photocatalysts were characterized by field emission scanning electron microscopy (FESEM), energy dispersive X-ray analysis (EDX), transmission electron microscopy (TEM), Fourier transform infrared spectroscopy (FTIR), X-ray diffraction spectroscopy (XRD), diffuse reflectance ultraviolet-visible spectroscopy (DR UV–Vis), Brunauer–Emmett–Teller surface area analysis, X-ray Fluorescence Spectroscopy (XRF) and photoluminescence spectroscopy (PL). The morphology of the samples was examined using FESEM–EDX (JEOL JED-2300) and TEM (JEOL JEM-2100, 200 kV). The FTIR spectra of the samples were obtained using a Perkin–Elmer spectrometer at a range of 400–4000 cm^{-1}. XRD experiments were carried out at room temperature using a Bruker AXS D8 Automatic Powder Diffractometer with Cu K_α radiation (λ = 1.5406 Å, 40 kV, 30 mA) to identify the crystal phase of the samples. The DR UV–Vis spectra were recorded on a UV–Vis–NIR spectrophotometer (Perkin Elmer Lambda 35) ranging from 200 to 800 nm at room temperature. PL spectra of samples were obtained on a Perkin–Elmer LS 55 luminescence spectrometer with 150 W Xe lamp, excitation at 355 nm. The surface area of the samples was determined by single point BET method. The BET surface area was measured on a Micromeritics ASAP 2010 with the gas composition of 30% N_2 and 70% He. XRF measurements were performed by a Rigaku EDXRF (Japan) spectrometer.

Photocatalytic testing

Photocatalytic testing of the catalysts prepared in the photodegradation of imazalil sulphate pesticide were performed at room temperature for 5 h under UV irradiation by using a 6 W UV lamp (Spectroline® ENF-260 C/FE) with the wavelength peak at 365 nm. The reaction mixture containing imazalil sulphate (100 mL, 15 mg L^{-1}) and catalyst (50 mg) was put into a simple degradation box and magnetically stirred throughout the degradation process. For the first 1 h, the suspension was left to reach complete adsorption–desorption equilibrium in dark condition. After 1 h, 10 mL of the solution was taken out and labeled as the initial time (t_0) of the degradation process. The UV lamp was switched on to irradiate the sample over a 5 h period. Samples were taken out using a 10 mL plastic syringe at the different time interval (1, 2, 3, 4 and 5 h) after irradiation and then filtered using a milipore membrane syringe filter of 0.45 µm in order to remove the photocatalyst particles. The degraded samples were measured using a UV–Visible spectrophotometer (Perkin Elmer Lambda 25) and the percentage of photodegradation was calculated.

RESULTS AND DISCUSSION

Physicochemical properties of Ag@TiO_2 and Ag/TiO_2 microspheres

FESEM images of Ag@TiO_2 and Ag/TiO_2 microspheres are shown in Fig. 2. It can be seen from the Fig. 2(a) that the synthesized particles are spherical in shape with an average diameter of about 536 nm. The white arrow in Fig. 2(a) shows partly broken sphere, thus confirming that the spheres are hollow inside. Fig. 2(b) shows Ag/TiO_2 spheres of about 670 nm in average diameter with a rough surface.

TEM image shown in Fig. 3(a) displays the core–shell structure of Ag@TiO_2 particles. It can be seen that the TiO_2 layer thickness is around 63 nm. The Ag nanoparticles can be clearly observed from the TEM image, as labeled by the white circles. It can be concluded that Ag@TiO_2 core–shell particles have been successfully fabricated. The TEM image of hollow anatase TiO_2 after Ag loading is given in Fig. 3(b). The presence of Ag nanoparticles deposited on hollow anatase TiO_2 can be clearly observed in the TEM image in Fig. 3(b). It can be observed that the Ag@TiO_2 spheres have larger Ag nanoparticles than Ag/TiO_2 because the high temperature during the calcination process provides sufficient energy for the growth of Ag particles. In addition, HRTEM images of the Ag@ TiO_2 and Ag/TiO_2 particles are shown in Figs. 3(c) and (d), in which the crystal lattice of TiO_2 and Ag can be identified. Lattice fringes with a lattice spacing of 0.35 and 0.24 nm

correspond to the (1 0 1) plane of anatase TiO_2 and Ag (1 1 1) plane, respectively.

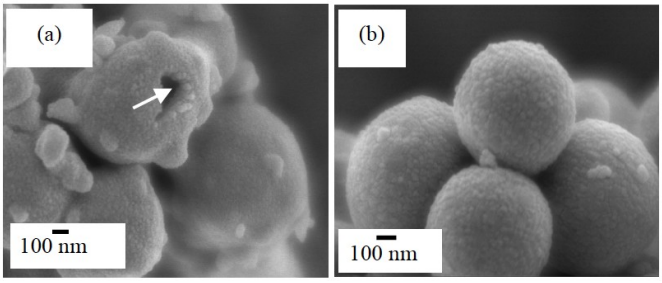

Fig. 2 FESEM images of (a) Ag@TiO_2 and (b) Ag/TiO_2 microspheres.

Further information on the elemental composition of the samples can be provided by EDX analysis. Fig. 4 shows the EDX spectrum of synthesized Ag@TiO_2 while the elemental composition of Ag@TiO_2 sample is summarized in Table 1. The EDX results confirmed the presence of Ti, O and Ag elements in the microspheres. The spectrum (Fig. 5) shows that Ag/TiO_2 microspheres consist of Ti, O and Ag elements with the corresponding percentages given in Table 2. The distribution of Ag in heterostructure was confirmed by the EDX elemental mapping as shown in Fig. 6. The EDX elemental mapping clearly shows the presence of Ag particles on TiO_2, which should correspond to the darker small spots in HRTEM image (Fig. 3(d)).

The FTIR spectrum of the Ag@C microspheres is shown in Fig. 7(a). The bands at 3119, 1707, 1605, 1190 and 797 cm^{-1} are attributed to the vibrations of ─OH, C═O, C═C, C─O and aromatic C─H out-of-plane bending, respectively. The presence of water is supported by the OH stretching mode peak appearance at 3119 cm^{-1}. The FTIR spectrum of Ag@TiO_2 anatase TiO_2 microspheres (Fig. 7(b)) shows a peak at about 3334 cm^{-1} and an absorption band around 1643 cm^{-1}, which are assigned to the vibrations of the surface adsorbed H_2O and Ti─OH bonds (Li *et al.*, 2007a). The broad band at 507–873 cm^{-1} originated from the TiO_2. The peak at 784 cm^{-1} is assigned to the symmetric O─Ti─O stretching while the peak at 595 cm^{-1} is due to the vibration of Ti─O bond (Nur, 2006). This confirms the formation of the inorganic shell and the removal of the organic components. The FTIR spectrum of Ag/TiO_2 particles is shown in Fig. 7(c) and shows similar peaks with Ag@TiO_2 microspheres.

XRD analysis was applied to determine the crystalline phase of the synthesized samples. The diffractogram shown in Fig. 8(a) shows the anatase peaks of TiO_2 at 2θ value of 25.3 (1 0 1), 37.9 (0 0 4), 48.0 (2 0 0), 54.0 (1 0 5), 55.1 (2 1 1) and 62.8° (2 0 4) (ICDD No. 04-0477). Apart from that, broadened diffraction peaks at 2θ values of 38.1, 44.2 and 64.1° are also observed. These peaks match with the (1 1 1), (2 0 0) and (2 2 0) crystal planes of face-centred cubic Ag (ICDD No. 01-071-4613). As the diffraction peak of the Ag (1 1 1) crystal plane is very near to that of the TiO_2 (0 0 4) plane, overlapping of the peaks occurred (Ong *et al.*, 2013). The XRD pattern of the Ag/TiO_2 particles is shown in Fig. 8(b). From Fig. 6, it can be seen that the XRD patterns of the Ag/TiO_2 and Ag@TiO_2 microspheres obtained are similar, although the crystallite growth of hollow TiO_2 in the Ag/TiO_2 somewhat hindered by the presence of Ag (Fig. 8(b)). Besides that, Scherrer's equation (Eq. (1)) was used to determine the crystallite size of the samples.

$$D = K\lambda / \beta \cos\theta \quad (1)$$

Where D is the crystallite size of the catalyst, λ is the X-ray

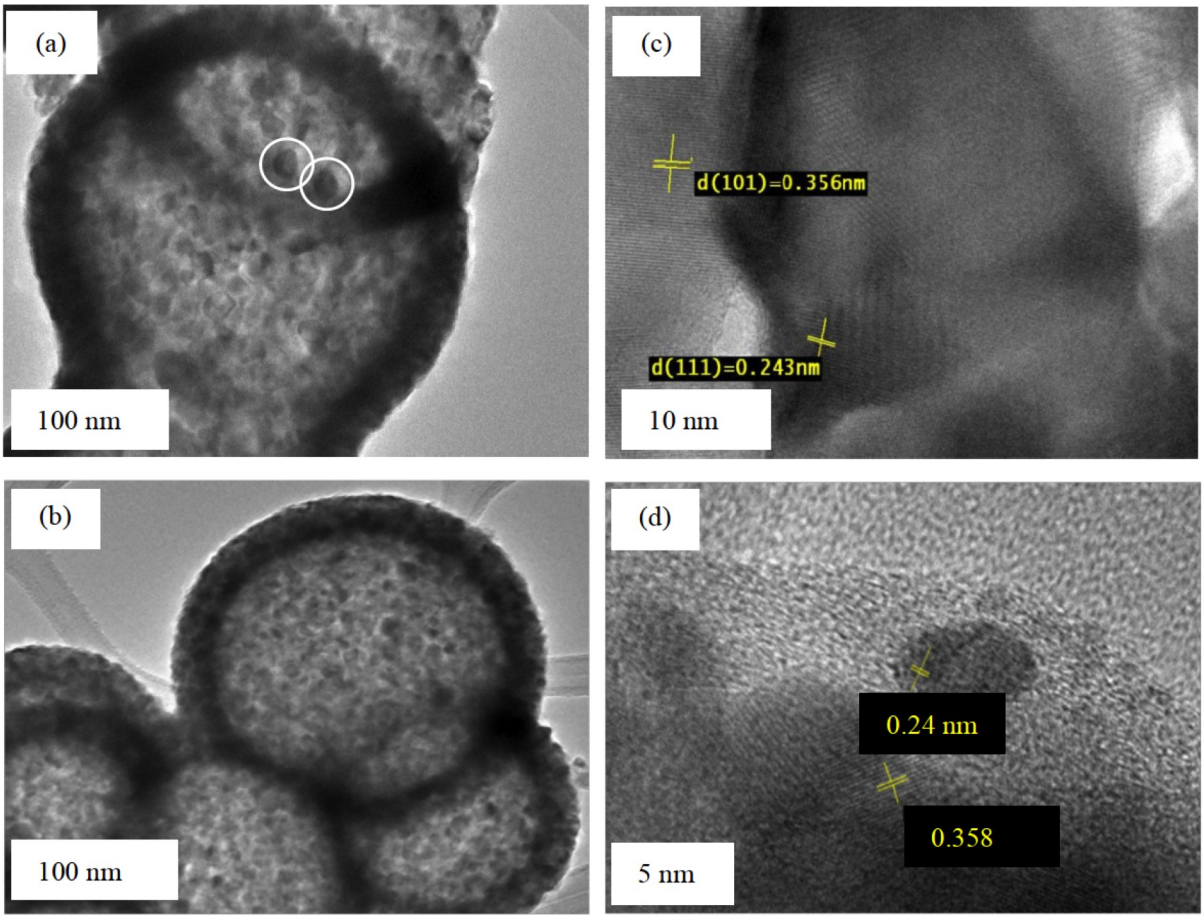

Fig. 3 TEM images of (a) TiO_2@Ag, (b) Ag/TiO_2 and (c, d) HRTEM images of Ag@TiO_2 and Ag/TiO_2, respectively.

wavelength (1.54 Å), β is the full width at half maximum (FWHM) of the diffraction peak (radian), K is a coefficient (0.89) and θ is the diffraction angle at the maximum peak. The crystallite size of the TiO_2 in the $Ag@TiO_2$ and Ag/TiO_2 estimated from their diffraction peaks width is 23.82 and 13.83 nm, respectively. The observed result is in good agreement with the obtained result from the TEM analysis and confirmed that the particles were composed of silver and anatase TiO_2.

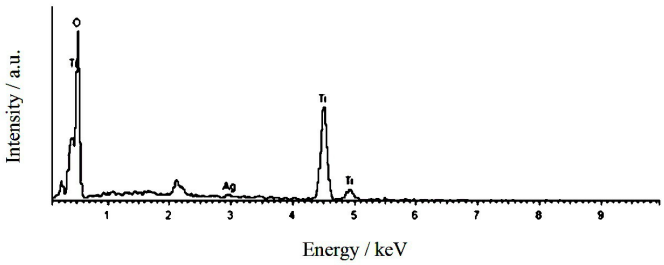

Fig. 4 EDX spectrum of $Ag@TiO_2$ sample.

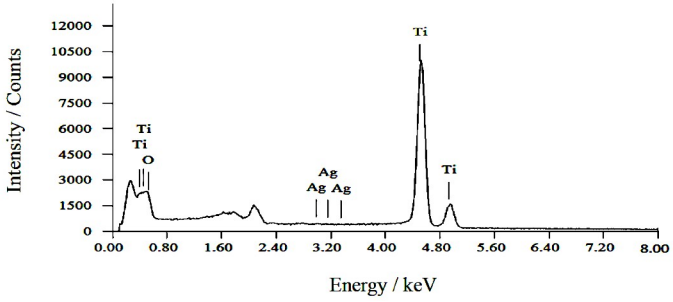

Fig. 5 EDX spectrum of Ag/TiO_2 microspheres.

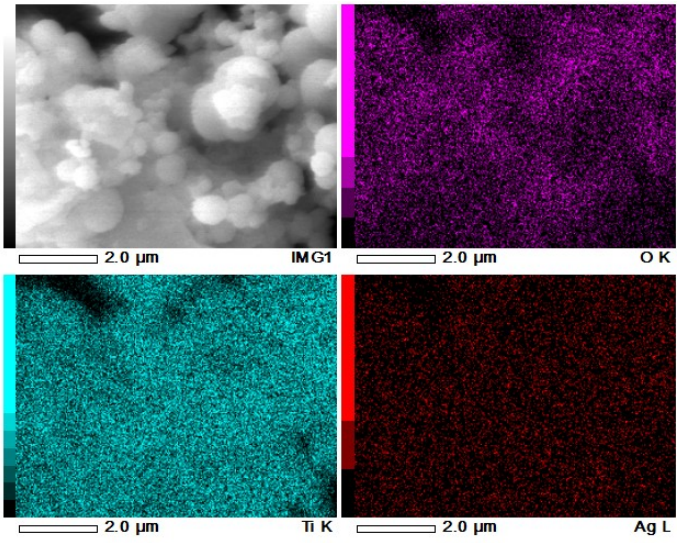

Fig. 6 EDX mapping of Ag/TiO_2 photocatalyst.

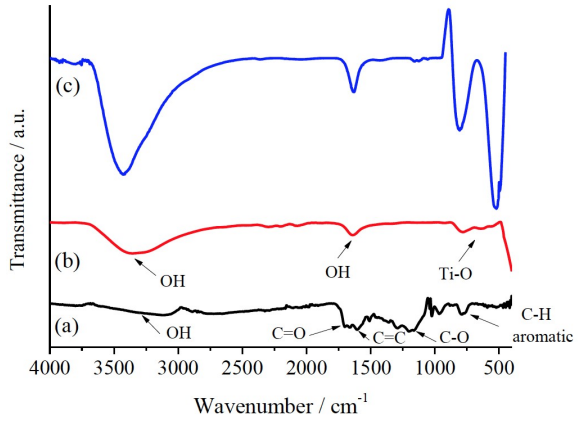

Fig. 7 FTIR spectra of (a) Ag@C microspheres, (b) $Ag@TiO_2$, and (c) Ag/TiO_2 particles.

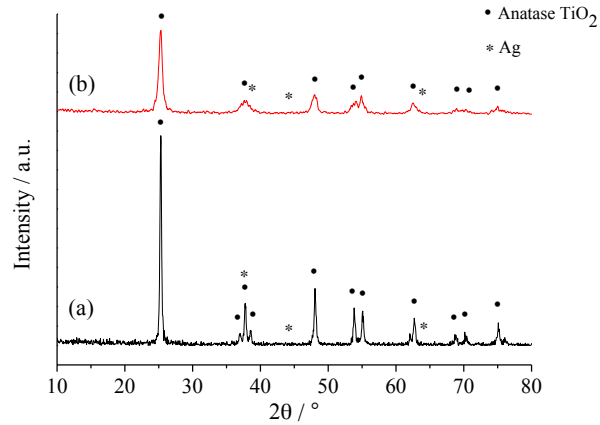

Fig. 8 XRD patterns of (a) $Ag@TiO_2$ and (b) Ag/TiO_2 microspheres.

Fig. 9 shows the DR UV–Vis spectra of the hollow anatase TiO_2, $Ag@TiO_2$, and Ag/TiO_2 microspheres. The onset of the absorption edge for hollow anatase TiO_2 sample is at $\lambda \approx 400$ nm. It is observed that the absorption spectra of $Ag@TiO_2$ and Ag/TiO_2 photocatalysts are obviously different from that of hollow anatase TiO_2. The weak peak observed at around λ = 404–650 nm is due to the surface plasmon absorption of electrons in Ag nanoparticles (Linic *et al.*, 2011; Scirè *et al.*, 2009; Cozzoli *et al.*, 2004). If the typical plasmon peak of Ag colloidal nanoparticles (Lee *et al.*, 2008b), which appears at $\lambda \approx$ 400–420 nm, is compared with those of $Ag@TiO_2$ and Ag/TiO_2 microspheres, a large red shift can be clearly observed. This behaviour can be related to a change in the metal particle size, where decreasing the size will result in a shift to the UV region (Albiter *et al.*, 2013). However, it has also been explained in terms of a strong interaction between metallic silver and TiO_2 (Jiang *et al.*, 2012; Zhang *et al.*, 2012; Ismail, 2012; Zhang *et al.*, 2011d; Liga *et al.*, 2011; Wodka *et al.*, 2010; Ashkarran *et al.*, 2011; Liang *et al.*, 2011; Xie *et al.*, 2010; Awazu *et al.*, 2008; Kubo and Tatsuma, 2006). The energy band gap of crystalline semiconductors can be calculated using the following equation:

$$\alpha h v = A (hv\text{-}E_g)^n \quad (2)$$

Where α is the absorption coefficient, h is Planck constant, v is the incident light frequency, A is a constant, E_g is the band gap and n depends on the nature of the transitions. The transitions may have values of 1/2, 2, 3/2 and 3, which correspond to allowed direct, allowed indirect, forbidden direct and forbidden indirect transitions, respectively. In TiO_2, n = 2 is usually considered. Experimental

diffuse reflectance data cannot be used directly to measure the absorption coefficients (α) because of scattering contributions to the reflectance spectra. Scattering coefficient depends weakly on the energy and Kubelka-Munk function ($F(R_\infty)$), (R_∞ is the diffuse reflectance) can be considered to be proportional to the absorption coefficient within the narrow range of energy containing the absorption edge features. In such way, the determination of the absorption edge energy can be estimated from the $(F(R_\infty)\cdot h\nu)^{1/n}$ versus $h\nu$ plot. In particular, the experimental band gap value can be obtained from the x-intercept of the straight tangent line to this plot. The indirect band gap energies (E_g) of the hollow anatase TiO_2, Ag@TiO_2, and Ag/TiO_2 are estimated to be approximately 3.16, 3.07 and 3.01 eV, respectively, (Fig. 10). These results indicate that the band gap energy of Ag@TiO_2 and Ag/TiO_2 was lower than that of hollow anatase TiO_2.

Table 1 Chemical composition of the Ag@TiO_2 from EDX analysis.

Element	Weight %
Titanium	55.22
Oxygen	44.04
Silver	0.74

Table 2 Weight percentage of Ti, O and Ag of Ag/TiO_2 microspheres.

Element	Weight %
Titanium	85.66
Oxygen	13.68
Silver	0.66

Fig. 11 shows the photoluminescence spectra of hollow anatase TiO_2, Ag@TiO_2, and Ag/TiO_2 particles. It can be seen that the PL spectrum of the hollow TiO_2 is more intense than the spectra of Ag@TiO_2 and Ag/TiO_2 samples. The decrease in the intensity may be due to the capturing of the photoinduced electron by Ag, thus inhibiting recombination of electron–hole pairs. The lower PL intensity of the Ag/TiO_2 sample clearly implies lower recombination rate (Liqiang *et al.*, 2006; Hirakawa and Kamat, 2004a; Chen *et al.*, 2007).

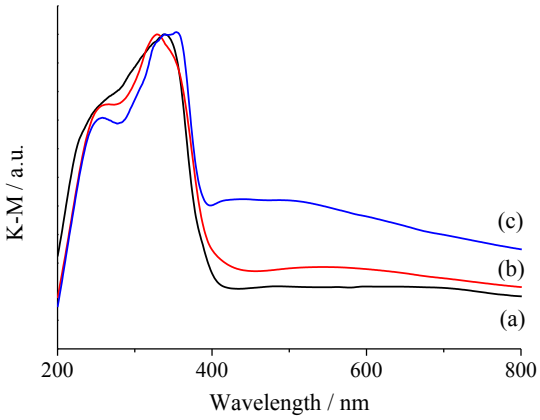

Fig. 9 DR UV–Vis spectra for (a) hollow anatase TiO_2, (b) Ag@TiO_2, and (c) Ag/TiO_2.

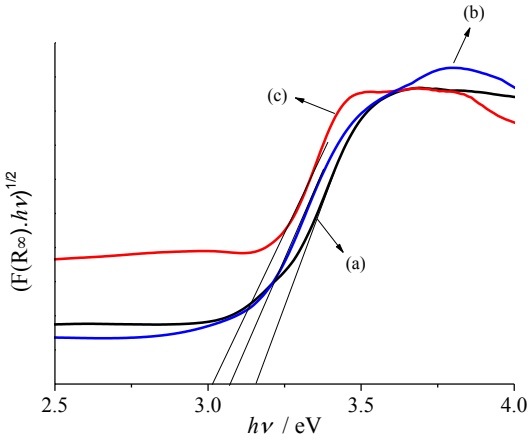

Fig. 10 Band gap evaluation for linear dependence of $(F(R_\infty).h\nu)^{1/2}$ versus photon energy for (a) hollow anatase TiO_2, (b) Ag@TiO_2, and (c) Ag/TiO_2.

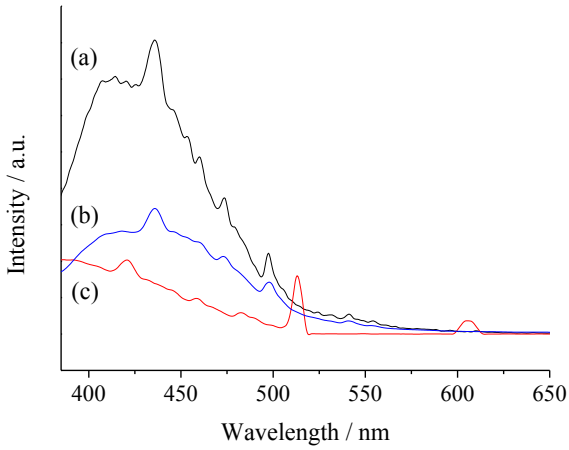

Fig. 11 Photoluminescence spectra of (a) hollow anatase TiO_2, (b) Ag@TiO_2 and (c) Ag/TiO_2 particles.

From the single point BET measurement, the specific surface areas are 23.26 $m^2\ g^{-1}$ for hollow anatase TiO_2, 15.22 for Ag@TiO_2 and 22.29 $m^2\ g^{-1}$ for $Ag_{(out)}$/hollow anatase TiO_2. When Ag nanoparticles were loaded onto the TiO_2, aiming at improving the photocatalytic performance, the surface area value of the hollow anatase TiO_2 remained unchanged even after Ag loading, probably due to the small amount of Ag deposited on the surface of TiO_2. The surface area of Ag@TiO_2 sample was less than that of the hollow anatase TiO_2, which might be due to the fact that the particles aggregated and formed bigger particles.

The amount of Ag in Ag@TiO_2 and Ag/TiO_2 samples was determined by XRF measurement. Table 3 and 4 illustrate Ag content in the prepared samples. Experimental Ag mass % measured by XRF technique is in good agreement with the calculated one, revealing the effectiveness of the current preparation methods.

Table 3 Elemental analysis by XRF for Ag@TiO_2 microspheres.

Component	Mass / %
Si	0.1
TiO_2	65.3
Ti	33.3
Ag	1.3
Mg	0.1
Al	0.1

Table 4 Elemental analysis by XRF for Ag/TiO_2 microspheres.

Component	Mass / %
Si	0.1
TiO_2	98.4
Ag	1.4
Mg	0.1
Al	0.1

Evaluation of photocatalytic activity

The photocatalytic activity of Ag modified hollow anatase TiO_2 microspheres in the environment was tested out in the photodegradation of imazalil sulphate and its imazalil sulphate photodegradation efficiency was compared with that of commercial TiO_2. The photodegradation efficiency was calculated using the Eq. (3).

$$\text{Photodegradation efficiency (\%)} = (1- C_t/C_0) \times 100 \qquad (3)$$

Where C_0 is the concentration of the compound before illumination and C_t is the concentration of solution after time t. Fig. 12 shows the photodegradation efficiency of imazalil sulphate. The photodegradation efficiency was in the following order: Ag/TiO_2 > hollow anatase TiO_2 > $Ag@TiO_2$ > commercial anatase TiO_2. The highest efficiency was shown by Ag/TiO_2 photocatalyst. 5 h of irradiation resulted in degradation of 27.9% for imazalil sulphate. From Fig. 12, it can be seen that the presence of Ag nanoparticles on the surface of hollow TiO_2 gave a more efficient photodegradation than the other photocatalysts, which demonstrates the efficiency of Ag nanoparticles in reducing the recombination rate of the electron-hole pair. Even though the prepared photocatalyst contains Ag in the metallic form, it can act as an electron sink (Wang *et al.*, 2013). When the reaction mixture is irradiated by UV, the photoexcited electrons from the valence band of TiO_2 gets captured by the Ag, allowing the generated hole to decompose the pesticides (Chiarello *et al.*, 2008; Wang *et al.*, 2013). Electron migration from the conduction band of TiO_2 to the metallic Ag particles is feasible since the Fermi level of TiO_2 is higher than that of Ag metal (Wang *et al.*, 2013). When the quantity of Ag is little and the photogenerated electrons effectively migrate to Ag, better separation of electrons and holes would be accomplished. The role of Ag is to increase separation of the electron-hole pair, decreasing recombination rate of the electron-hole pair and in turn, enhanced the photocatalytic efficiency of the Ag/TiO_2 photocatalyst.

Additionally, the Ag nanoparticles can impact photoluminescence properties of TiO_2. photoluminescence phenomenon is a kind of photophysical process, and the photocatalytic reaction is a kind of photochemical process (Liqiang *et al.*, 2006). The photoluminescence and photocatalytic processes are nearly associated with dynamic behaviours of photoinduced charge carriers of TiO_2. Consequently, there are definite relationship between photoluminescence and photocatalysis, and the inherent relationship between photoluminescence intensity and photocatalytic performance can be shown on the basis of photoluminescence characteristics (Liqiang *et al.*, 2006). Photoluminescence may be effectively utilized to screen recombination and generally, low-intensity photoluminescence signals indicate lower recombination rates (Liqiang *et al.*, 2006).

According to Fig. 13, it can be seen that the lowest photoluminescence intensity of the sample corresponds to the highest photocatalytic efficiency. This is because the lower the photoluminescence intensity, the stronger the capacity of the Ag to capture photoinduced electrons, the higher the separation rate of photoinduced electrons and holes, and the higher the photocatalytic efficiency.

In other words, the Ag nanoparticles have a great effect on the separation and recombination processes of photoinduced charge carriers of Ag/TiO_2 sample and can further influence the photoluminescence performance. Therefore, it can be suggested that the photocatalytic efficiency of samples can be evaluated by means of photoluminescence measurements.

It is also proposed that Ag is more efficient when it comes to photodegradation of molecules with smaller particles (9–20 nm particle size of Ag on the TiO_2's surface compared with 45 nm the average size of Ag particles inside the hollow TiO_2 sample). Smaller particles, implying a larger contact area between Ag and TiO_2, were found to result in better charge separation and gave better photodegradation performance. This is in agreement with the results shown in Fig. 12.

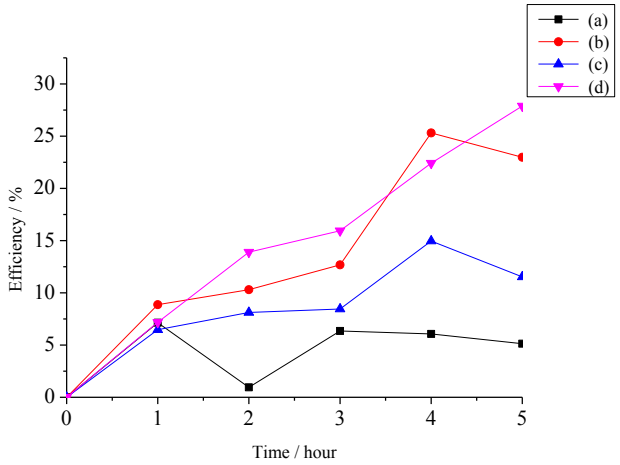

Fig. 12 Graph for the photocatalytic degradation of imazalil sulphate pesticide in aqueous solution in the presence of (a) commercial anatase TiO_2, (b) hollow anatase TiO_2, (c) $Ag@TiO_2$ and (d) Ag/TiO_2.

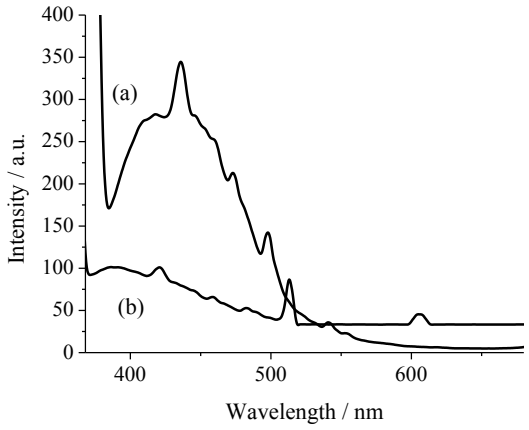

Fig. 13 Photoluminescence spectra of (a) $Ag@TiO_2$ and (b) Ag/TiO_2.

CONCLUSION

Hollow anatase TiO_2 containing Ag, in the different location, has been successfully synthesized. This was proven by the images obtained using TEM. Apart from that, the existence of Ag was also confirmed by XRF and EDX. DR UV–Vis spectra showed the existence of absorbance peak for Ag at around 404–650 nm. The Ag's particles size was measured by TEM. The results showed that the size of Ag particles inside the hollow anatase TiO_2 sample was larger (45 nm) than its particles size when it was located outside (9–20 nm). The photocatalytic efficiency of the hollow anatase TiO_2 and hollow anatase TiO_2 containing Ag was evaluated by the degradation of imazalil sulphate pesticide under UV light irradiation. The Ag/TiO_2 particles exhibited the highest performance in the photodegradation of the aqueous phase of imazalil sulphate pesticide (35.9%) compared

with the other photocatalysts used in this work. The higher photocatalytic efficiency of Ag/TiO_2 particles is related to the role of Ag on the surface of hollow anatase TiO_2 particles. The deposition of Ag onto the surface of hollow anatase TiO_2 is shown to be beneficial in increasing the efficiency of pesticide photocatalytic degradation. Ag nanoparticles can act as an electron acceptor centre, allowing electron and hole pair separation and hence leading to the overall improved photocatalytic efficiency of hollow anatase TiO_2.

ACKNOWLEDGEMENT

This work was financially supported by the Universiti Teknologi Malaysia under the Research University Grant and Ministry of Higher Education Malaysia.

REFERENCES

Abou El-Nour, K.M.M., Eftaiha, A., Al-Warthan, A., Ammar, R.A.A. 2010. Synthesis and applications of silver nanoparticles. *Arabian J. Chem*. 3, 135-140.

Albiter, E., Hai, Z., Alfaro, S., Remita, H., Valenzuela, M.A., Colbeau-Justin, C. 2013. A comparative study of photo-assisted deposition of silver nanoparticles on TiO_2. *J. Nanosci. Nanotechnol.* 13, 4943-4948.

Ashkarran, A.A., Aghigh, S.M., kavianipour, M., Farahani, N. J. 2011. Visible light photo-and bioactivity of Ag/TiO_2 nanocomposite with various silver contents. *Curr. Appl Phys.* 11, 1048-1055.

Awazu, K., Fujimaki, M., Rockstuhl, C., Tominaga, J., Murakami, H., Ohki, Y., Yoshida, N., Watanabe, T. 2008. A plasmonic photocatalyst consisting of silver nanoparticles embedded in titanium dioxide. *J. Am. Chem. Soc.* 130, 1676-1680.

Baharvand, A., Ali, R., Yusof, A.M., Ibrahim, A. N., Chandren, S., Nur, H. 2014. Preparation of Anatase Hollow TiO_2 Spheres and Their Photocatalytic Activity in the Photodegradation of Chlorpyrifos. *J. Chinese Chem. Soc*. 61, 1211-1216.

Behnajady, M. A., Modirshahla, N., Shokri, M., Rad, B. 2008. Enhancement of photocatalytic activity of TiO_2 nanoparticles by Silver doping: Photodeposition versus liquid impregnation methods. *Global Nest J*. 10, 1-7.

Chan, S. C., Barteau, M.A. 2005. Preparation of highly uniform Ag/TiO_2 and Au/TiO_2 supported nanoparticle catalysts by photodeposition. *Langmuir* 21, 5588-5595.

Chatterjee, D., Mahata, A. 2002. Visible light induced photodegradation of organic pollutants on dye adsorbed TiO_2 surface. *J. Photochem. Photobiol. A* 153, 199-204.

Chen, H.W., Ku, Y., Kuo, Y.L. 2007. Photodegradation of o-cresol with Ag deposited on TiO_2 under visible and UV light irradiation. *Chem. Eng. Technol*. 30, 1242-1247.

Chiarello, G.L., Selli, E., Forni, L. 2008. Photocatalytic hydrogen production over flame spray pyrolysis-synthesised TiO_2 and Au/TiO_2. *Appl. Catal. B* 84, 332-339.

Cozzoli, P. D., Comparelli, R., Fanizza, E., Curri, M.L., Agostiano, A., Laub, D. 2004. Photocatalytic synthesis of silver nanoparticles stabilized by TiO_2 nanorods: A semiconductor/metal nanocomposite in homogeneous nonpolar solution. *J. Am. Chem. Soc.* 126, 3868-3879.

Grabowska, E., Zaleska, A., Sorgues, S., Kunst, M., Etcheberry, A., Colbeau-Justin, C., Remita, H. 2013. Modification of titanium(IV) dioxide with small silver nanoparticles: Application in photocatalysis. *J. Phys, Chem. C* 117, 1955-1962.

Herrmann, J.-M. 1999. Heterogeneous photocatalysis: fundamentals and applications to the removal of various types of aqueous pollutants. *Catal. Today*. 53, 115-129.

Hirakawa, T., Kamat, P.V. 2004a. Photoinduced electron storage and surface plasmon modulation in $Ag@TiO_2$ clusters. *Langmuir* 20, 5645-5647.

Hirakawa, T., Kamat, P.V. 2004b. Photoinduced electron storage and surface plasmon modulation in $Ag@TiO_2$ clusters. *Langmuir* 20, 5645-5647.

Hirakawa, T., Kamat, P.V. 2005. Charge separation and catalytic activity of $Ag@TiO_2$ core−shell composite clusters under UV−irradiation. *J. Am. Chem. Soc.* 127, 3928-3934.

Ismail, A. A. 2012. Facile synthesis of mesoporous Ag-loaded TiO_2 thin film and its photocatalytic properties. *Microporous Mesoporous Mater.* 149, 69-75.

Jang, S.-R., Vittal, R., Lee, J., Jeong, N., Kim, K.-J. 2006. Linkage of N_3 dye to N_3 dye on nanocrystalline TiO_2 through trans-1,2-bis(4-pyridyl)ethylene for enhancement of photocurrent of dye-sensitized solar cells. *Chem. Commun*. 103-105.

Jiang, L., Zhou, G., Mi, J., Wu, Z. 2012. Fabrication of visible-light-driven one-dimensional anatase TiO_2/Ag heterojunction plasmonic photocatalyst. *Catal. Commun*. 24, 48-51.

Kondo, Y., Yoshikawa, H., Awaga, K., Murayama, M., Mori, T., Sunada, K., Bandow, S., Iijima, S. 2007. Preparation, photocatalytic activities, and dye-sensitized solar-cell performance of submicron-scale TiO_2 hollow spheres. *Langmuir* 24, 547-550.

Kubo, W., Tatsuma, T. 2006. Mechanisms of photocatalytic remote oxidation. *J. Am. Chem. Soc*. 128, 16034-16035.

Lee, M.-K., Kim, T.G., Kim, W., Sung, Y.-M. 2008b. Surface plasmon resonance (SPR) electron and energy transfer in noble metal–zinc oxide composite nanocrystals. *J. Phys. Chem. C* 112, 10079-10082.

Lenzi, G.G., Fávero, C.V.B., Colpini, L.M.S., Bernabe, H., Baesso, M.L., Specchia, S., Santos, O. A. A. 2011. Photocatalytic reduction of Hg(II) on TiO_2 and Ag/TiO_2 prepared by the sol-gel and impregnation methods. *Desalination*. 270, 241-247.

Li, H., Bian, Z., Zhu, J., Huo, Y., Li, H., Lu, Y. 2007a. Mesoporous Au/TiO_2 nanocomposites with enhanced photocatalytic activity. *J. Am. Chem. Soc*. 129, 4538-4539.

Li, H., Bian, Z., Zhu, J., Zhang, D., Li, G., Huo, Y., Li, H., Lu, Y. 2007b. Mesoporous Titania Spheres with Tunable Chamber Stucture and Enhanced Photocatalytic Activity. *J. Am. Chem. Soc*. 129, 8406-8407.

Liang, Y.-C., Wang, C.-C., Kei, C. -C., Hsueh, Y.-C., Cho, W.-H., Perng, T.-P. 2011. Photocatalysis of Ag-loaded TiO_2 nanotube arrays formed by atomic layer deposition. *J. Phys. Chem. C* 115, 9498-9502.

Liga, M.V., Bryant, E.L., Colvin, V.L., Li, Q. 2011. Virus inactivation by silver doped titanium dioxide nanoparticles for drinking water treatment. *Water Res.* 45, 535-544.

Linic, S., Christopher, P., and Ingram, D.B. 2011. Plasmonic-metal nanostructures for efficient conversion of solar to chemical energy. *Nat. Mater*. 10, 911-921.

Liqiang, J., Yichun, Q., Baiqi, W., Shudan, L., Baojiang, J., Libin, Y., Wei, F., Honggang, F., Jiazhong, S. 2006. Review of photoluminescence performance of nano-sized semiconductor materials and its relationships with photocatalytic activity. *Sol. Energy Mater. Sol. Cells* 90, 1773-1787.

Nur, H. 2006. Modification of titanium surface species of titania by attachment of silica nanoparticles. *Mater. Sci. Eng. B* 133, 49-54.

Ong, W. L., Gao, M., and Ho, G. W. 2013. Hybrid organic PVDF-inorganic M-rGO-TiO_2 (M = Ag, Pt) nanocomposites for multifunctional volatile organic compound sensing and photocatalytic degradation-H_2 production. *Nanoscale* 5, 11283-11290.

Pastoriza-Santos, I., Koktysh, D.S., Mamedov, A.A., Giersig, M., Kotov, N.A., Liz-Marzán, L.M. 2000. One-pot synthesis of $Ag@TiO_2$ core-shell nanoparticles and their layer-by-layer assembly. *Langmuir* 16, 2731-2735.

Scirè, S., Crisafulli, C., Giuffrida, S., Mazza, C., Riccobene, P.M., Pistone, A., Ventimiglia, G., Bongiorno, C., Spinella, C. 2009. Supported silver catalysts prepared by deposition in aqueous solution of Ag nanoparticles obtained through a photochemical approach. *Appl. Catal A* 367, 138-145.

Sclafani, A., Herrmann, J.-M. 1998. Influence of metallic silver and of platinum-silver bimetallic deposits on the photocatalytic activity of titania (anatase and rutile) in organic and aqueous media. *J. Photochem. Photobiol. A* 113, 181-188.

Seery, M.K., George, R., Floris, P., Pillai, S.C. 2007. Silver doped titanium dioxide nanomaterials for enhanced visible light photocatalysis. *J. Photochem. Photobiol. A* 189, 258-263.

Sharma, V.K., Yngard, R.A., Lin, Y. 2009. Silver nanoparticles: Green synthesis and their antimicrobial activities. *Adv. Colloid Interface Sci*. 145, 83-96.

Subrahmanyam, A., Biju, K. P., Rajesh, P., Kumar, K.J., Kiran, M.R. 2012. Surface modification of sol gel TiO_2 surface with sputtered metallic silver for Sun light photocatalytic activity: Initial studies. *Sol. Energ. Mater. Sol. Cells* 101, 241-248.

Subramanian, V., Wolf, E.E., Kamat, P.V. 2004. Catalysis with TiO_2/gold nanocomposites. Effect of metal particle size on the fermi level equilibration. *J Am. Chem. Soc*. 126, 4943-4950.

Tada, H., Kubo, Y., Akazawa, M., Ito, S. 1998. Promoting effect of SiO_x monolayer coverage of TiO_2 on the photoinduced oxidation of cationic surfactants. 14, 2936-2939.

Tao, A., Sinsermsuksakul, P., Yang, P. 2006. Polyhedral silver nanocrystals with distinct scattering signatures. *Angew. Chem. Int. Edit*. 45, 4597-4601.

Tom, R.T., Nair, A. S., Singh, N., Aslam, M., Nagendra, C., Philip, R., Vijayamohanan, K., Pradeep, T. 2003. Freely dispersible $Au@TiO_2$, $Au@ZrO_2$, $Ag@TiO_2$, and $Ag@ZrO_2$ core-shell nanoparticles: One-step synthesis, characterization, spectroscopy, and optical limiting properties. *Langmuir* 19, 3439-3445.

Ung, T., Liz-Marzán, L.M., Mulvaney, P. 1998. Controlled Method for Silica Coating of Silver Colloids. Influence of Coating on the Rate of Chemical Reactions. *Langmuir* 14, 3740-3748.

Wang, S., Qian, H., Hu, Y., Dai, W., Zhong, Y., Chen, J., Hu, X. 2013. Facile one-pot synthesis of uniform TiO_2-Ag hybrid hollow spheres with enhanced photocatalytic activity. *Dalton Trans*. 42, 1122-1128.

Wodka, D., Bielańska, E., Socha, R.P., Elżbieciak-Wodka, M., Gurgul, J., Nowak, P., Warszyński, P., Kumakiri, I. 2010. Photocatalytic activity of

titanium dioxide modified by silver nanoparticles. *ACS Appl. Mater. Interfaces* 2, 1945-1953.

Xie, K., Sun, L., Wang, C., Lai, Y., Wang, M., Chen, H., Lin, C. 2010. Photoelectrocatalytic properties of Ag nanoparticles loaded TiO_2 nanotube arrays prepared by pulse current deposition. *Electrochim. Acta* 55, 7211-7218.

Xu, M.-W., Bao, S.-J., and Zhang, X.-G. 2005. Enhanced photocatalytic activity of magnetic TiO_2 photocatalyst by silver deposition. *Mater. Lett*. 59, 2194-2198.

Yu, J., Liu, S., Yu, H. 2007b. Microstructures and photoactivity of mesoporous anatase hollow microspheres fabricated by fluoride-mediated self-transformation. *J. Catal*. 249, 59-66.

Zhang, H., Liang, C., Liu, J., Tian, Z., Wang, G., Cai, W. 2012. Defect-mediated formation of Ag cluster-doped TiO_2 nanoparticles for efficient photodegradation of pentachlorophenol. *Langmuir* 28, 3938-3944.

Zhang, S., Peng, F., Wang, H., Yu, H., Zhang, S., Yang, J., Zhao, H. 2011d. Electrodeposition preparation of Ag loaded N-doped TiO_2 nanotube arrays with enhanced visible light photocatalytic performance. *Catal. Commun*. 12, 689-693.

Zhou, J., Cheng, Y., Yu, J. 2011. Preparation and characterization of visible-light-driven plasmonic photocatalyst $Ag/AgCl/TiO_2$ nanocomposite thin films. *J. Photochem. Photobiol. A* 23, 82-87.

Zielińska, A., Kowalska, E., Sobczak, J.W., Łącka, I., Gazda, M., Ohtani, B., Hupka, J., Zaleska, A. 2010. Silver-doped TiO_2 prepared by microemulsion method: Surface properties, bio- and photoactivity. *Sep. Purif. Technol*. 72, 309-318.